RESEARCH ARTICLE | MARCH 05 2024

Measurement of residual elastic strain in rolled-up amorphous nanomembranes using nanobeam electron diffraction

Zhi Zheng ; Chang Liu ; Wenhao He ; Jiayuan Huang ; Jiachuo He ; Gaoshan Huang ; Yongfeng Mei ✉ ; Changlin Zheng ✉

Check for updates

CrossMark

View Online   Export Citation

20 March 2024 08:34:19

Measurement of residual elastic strain in rolled-up amorphous nanomembranes using nanobeam electron diffraction

View Online   Export Citation   CrossMark

Zhi Zheng,[1] (iD) Chang Liu,[1] (iD) Wenhao He,[2] (iD) Jiayuan Huang,[1] (iD) Jiachuo He,[2] (iD) Gaoshan Huang,[1,3,4] (iD)
Yongfeng Mei,[1,3,4,5,a)] (iD) and Changlin Zheng[2,a)] (iD)

AFFILIATIONS

[1]Department of Materials Science & State Key Laboratory of Molecular Engineering of Polymers, Fudan University,
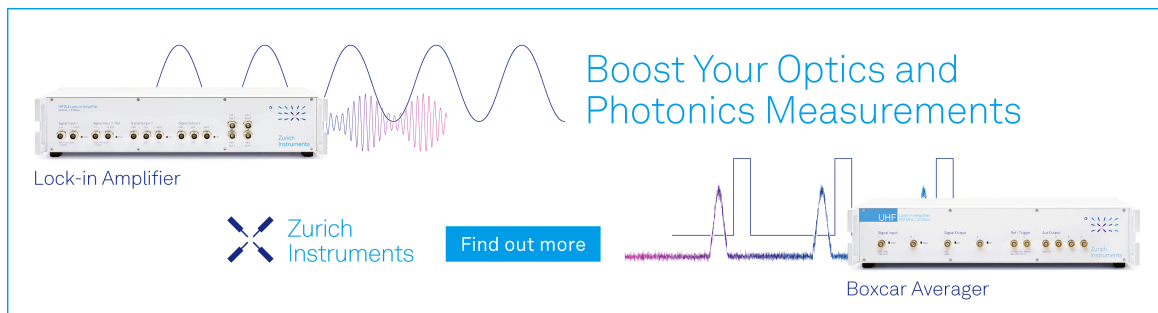Shanghai 200438, People's Republic of China
[2]Department of Physics & State Key Laboratory of Surface Physics, Fudan University, Shanghai 200438, People's Republic of China
[3]Yiwu Research Institute of Fudan University, Yiwu, Zhejiang 322000, People's Republic of China
[4]International Institute of Intelligent Nanorobots and Nanosystems, Fudan University, Shanghai 200438, People's Republic of China
[5]Shanghai Frontiers Science Research Base of Intelligent Optoelectronics and Perception, Institute of Optoelectronics,
Fudan University, Shanghai 200438, People's Republic of China

[a)]Authors to whom correspondence should be addressed: yfm@fudan.edu.cn and zcl@fudan.edu.cn

ABSTRACT

Amorphous nanomembranes play a crucial role in flexible electronics due to their ability to create intricate 3D structures through strain engineering. To better understand the formation of these structures, accurately mapping the local elastic strain distribution is essential. In this study, we conducted position-sensitive nanobeam electron diffraction investigations on various rolled-up amorphous nanomembranes. By analyzing the diffraction rings obtained from different locations on the amorphous samples, we extracted anisotropic structure information in reciprocal space and determined the local strain distributions in real space. Our analysis revealed that particle-assisted dry-released samples exhibited higher strain values than pure amorphous samples. This suggests that nanoparticles introduce additional strain through dewetting effects, thereby facilitating the formation of self-rolling 3D structures.

Flexible electronic devices can be bent, folded, stretched, or rolled without losing functionality.[1] They offer several advantages over conventional rigid electronic devices, including lightweight,[2] compactness,[3] conformability,[4] and versatility.[5–7] Amorphous materials play a crucial role in flexible electronics due to their unique mechanical properties to form complex 3D structures. They have been applied in various components of flexible electronic devices, including versatile, flexible substrates,[8,9] sensing layers,[10] and transistors.[11] The recent development of thin film technology and the increasing demand for multi-functional micro/nanodevices have led to a more dedicated fabrication and engineering of amorphous nanomembranes. This enables the creation of intricate 3D structures at smaller scales, facilitating the construction of advanced flexible systems. For instance, by exploiting the strain after nanomembrane deposition, 2D thin films can be folded or rolled into 3D structures. These structures, combining low-dimensional characteristics with unique mechanical features, have

been extensively utilized as innovative building blocks in various applications. They are not only applied in flexible electronics[5,12] but also extend to other areas such as energy storage,[13] optical resonators and metamaterial fibers,[14,15] microfluidics, biosensors, and self-propelled micromachines.[16,17] To further improve the performance and reduce the sizes of the devices, it is necessary to control the number of windings, diameters, and position of the rolled-up nanomembranes precisely. Prior research has demonstrated that many factors, including dissimilarities in thermal expansion between the sacrificial layer and deposited film, deposition rate, and stress changes during the deposition process, can impact the distribution of stress and strain and the ultimate conditions following release.[18] Therefore, it is essential to map the local elastic strain distributions with high spatial resolution to establish a correlation between strain distribution and the formation of 3D rolled-up amorphous nanomembrane structures.

20 March 2024 08:34:19

There has been a growing emphasis on studying local microscopic strain fields in materials in recent decades. Transmission electron microscopy (TEM) is frequently used to quantify strain distributions at the nanoscale because of its exceptional spatial resolution and precision.[19–25] For crystalline materials, it is feasible to directly examine the displacements of atoms from their original positions using atomic resolution TEM or scanning transmission electron microscopy (STEM).[26–28] Image analysis methodologies on atomically resolved images, such as geometric phase analysis,[29] peak finding,[19] and peak pairing,[30] have been well developed and applied to analyze strain distributions with picometer accuracy. More recently, strain mapping in TEM is also been performed in reciprocal space to achieve a large field of view.[31] This can be done by directly measuring the shift of Bragg diffraction disks using a fast pixelated electron detector in the scanning mode[32,33] or by creating strain-introduced geometric phase imaging using a Bragg diffraction beam in the dark-field electron holography.[34–36] In contrast to crystalline materials, probing the local elastic strain in amorphous materials is more challenging. This is because amorphous materials neither do show individual atom positions on high-resolution S/TEM images nor do they show discrete diffraction spots/disks in reciprocal space. Only limited attempts have been made to map the local strains in amorphous materials using S/TEM, such as measuring the mechanical response of the amorphous thin film under artificially induced strain[37] or strain distributions in metallic glasses.[38] The microscopic strain distribution in 3D rolled-up nanomembranes with complex residual strain states has not been extensively studied. This is primarily due to the challenges in measuring strain in amorphous materials with complex 3D nano-geometry.

This study investigates the residual strain distributions of 3D rolled-up amorphous nanomembranes using position-sensitive nanobeam electron diffraction (NBED). We extract the directions and strengths of local strain from the ellipticity of diffraction rings in reciprocal space. The rolled-up nanomembranes, composed of multiple layers of amorphous materials, are constructed using both wet-etching and dry-etching releasing techniques. We examine the characteristic diffused diffraction ring of corresponding amorphous materials and fit into an ellipse, from which the uniaxial tangential strain inside the cross section of the nanomembranes is calculated. Previous studies show the residual strain states in the rolled-up structures are different due to the presence of the metal nanoparticles.[39] Here, our investigations show that the presence of nanoparticles introduces additional strain through dewetting effects and promotes the formation of self-rolling 3D structures.

The amorphous nanomembrane structures are fabricated through a rolled-up technique, which involves the deposition of strained material layers and the subsequent release and relaxation. Dry-releasing and wet-etching processes are applied for comparison. Figure 1 shows the schematics of a typical sample preparation process and the experimental setup of NBED. The fabrication process is started by the deposition of amorphous SiO and SiO_2 layers [both ~5 nm in thickness, as labeled in Fig. 1(a)] via electron beam evaporation on a sacrificial layer (PMMA). The differences in the intrinsic atoms' distance in SiO and SiO_2 and their thermal expansion coefficients lead to a disparity in intrinsic strain between the two layers. A dry-release technique is applied to avoid liquid contamination.[39] Another layer of Pd thin film is then deposited at last on top of the nanomembranes to introduce additional stress. Then, the whole sample is treated by rapid thermal annealing (RTA) in N_2 environment to remove the sacrificial layer and trigger the dewetting process of the metal layer. Specifically, during RTA treatment, the metal (i.e., Pd) becomes fully molten and turns into densely distributed droplets on the nanomembrane surface. During the releasing and dewetting process, the films' intrinsic strain difference and the metal nanoparticles' surface tension contribute to the nanomembranes' rolling. Consequently, we can achieve rolled-up nanotubes decorated with Pd nanoparticles in large output, which can
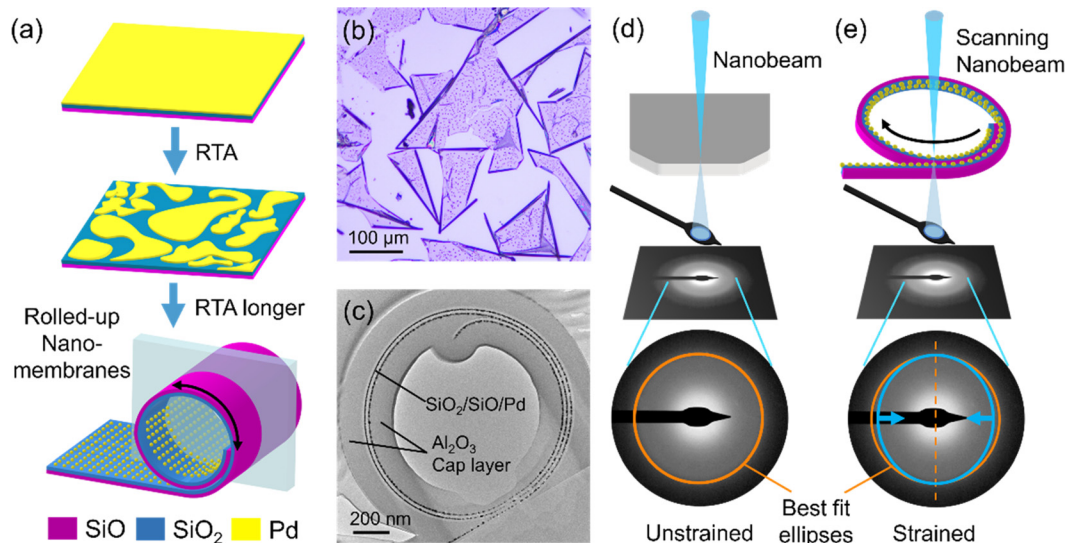
FIG. 1. Illustration of sample preparation and NBED strain mapping of multilayer rolled-up nanomembranes. (a) Schematics of sample fabrication using dry-releasing rolling with rapid thermal annealing treatment. The light blue-shaded part in the bottom panel illustrates the FIB cutting for the cross-sectional TEM samples. (b) Optical microscope images of the rolled-up samples. (c) Bright field cross-sectional TEM image of a FIB fabricated sample. (d) and (e) The NBED experiment schematics of unstrained and strained samples, respectively.

20 March 2024 08:34:19

be observed by light microscope and TEM as shown in Figs. 1(b) and 1(c). The rolled-up SiO/SiO$_2$ nanomembrane has a radius of ~600 nm (see Fig. S1). The TEM image in Fig. 1(c) shows the cross-sectional view of the rolled-up nanomembranes prepared by focused ion beam (FIB). To protect bilayer nanotubes from collapse or damage during FIB cutting and milling,[40] a cap layer of Al$_2$O$_3$ was deposited on the sample using atomic layer deposition.[41,42] This was done after the rolling process to ensure the residual strain distributions in the bilayer nanotubes were not significantly affected. In addition, we conducted the ALD growth of the Al$_2$O$_3$ at a temperature significantly lower than the rapid thermal annealing used for dry etching, which further minimally impacts the existing strain of the bilayer. We examined the diameter of the rolled-up nanomembranes with a light microscope and found no noticeable changes. As shown in Fig. 1(c), the Al$_2$O$_3$ grew symmetrically on both the inner and outer sides of the bilayer tubes, further reducing the potential to modify the strain distributions in the bilayers. The rolled-up amorphous Si$_3$N$_4$ nanomembrane was also made by the well-developed wet-etching process.[43–45] Briefly, a 40 nm thick Si$_3$N$_4$ layer is deposited with electron-beam evaporation onto a sacrificial Ge layer, which is then etched by H$_2$O$_2$, resulting in the rolling of Si$_3$N$_4$ nanomembrane with a radius of ~5.8 μm (Fig. S2). A cap layer of Al$_2$O$_3$ is also deposited for protection. The main differences between the two rolled-up samples are the presence of wet etchant and the metal nanoparticles at the surface, while both rolled-up nanomembranes show homogeneous radii and complete appearance without broken or crushed parts.

Due to the disordered nature of amorphous materials, direct atom identification or specific diffraction spots corresponding to periodically separated planes could not be acquired in TEM. Fortunately, the structure information is also encoded in the diffused diffraction ring in reciprocal space.[46] For the typical diffraction rings of amorphous materials, the radius of the diffraction ring reveals the bond length,[47–49] which is described by the radial distribution function (RDF) or pair distribution function (PDF).[50] According to the definition of uniaxial microscopic elastic strain, the elongation or compression (ΔL) with respect to the original interatomic distance (L_0), i.e., $\frac{\Delta L}{L_0}$, is the local atomic strain. Figures 1(d) and 1(e) illustrate the difference in reciprocal space (diffraction patterns) between the samples without and with residual strain, respectively. Here, we use nanobeam electron diffraction to measure strain in reciprocal space while preserving the spatial resolving ability in real space. The nanobeam diffraction pattern of the strain-free sample appears as a circle, with a peak-intensity radius described as q_0. In contrast, the strained sample exhibits a diffraction pattern in the shape of an ellipse. The position of the first diffused ring of the diffraction pattern, $q(\vartheta)$, is then varied as a function of the azimuthal angle ϑ in strained samples. When there is uniaxial compressive strain in amorphous materials, which corresponds to a decrease in the interatomic distance, it causes the diffraction pattern in reciprocal space to elongate along the strain direction. The total strain describes the amount of relative tensile or compressive deformation, quantized by $L' - L_0$, of amorphous materials in a certain region of interest (ROI),

$$\varepsilon(\vartheta) = \frac{q_0 - q(\vartheta)}{q_0}$$
$$= \frac{L' - L_0}{L_0}$$
$$= \varepsilon_\tau \cos^2(\vartheta) + 2\varepsilon_{\tau,r}\cos(\vartheta)\sin(\vartheta) + \varepsilon_r \sin^2(\vartheta), \quad (1)$$

where ε_τ, $\varepsilon_{\tau,r}$, and ε_r are defined as tangential strain (along the tangential direction of the tube), cross term, and normal strain, respectively. According to the bilayer rolling mechanism which is well developed with elastic energy theory and planar model,[51] the rolling behavior of a planar bilayer could be described quantitatively. The curvature, K, after rolling for the bilayer structure, can be estimated as follows:

$$K = \frac{1}{R} = \frac{6E_1 E_2 t_1 t_2 (t_1 + t_2)\left(\eta_1 \varepsilon_1^0 - \eta_2 \varepsilon_2^0\right)}{E_1^2 t_1^4 + E_2^2 t_2^4 + 2E_1 E_2 t_1 t_2 \left(2t_1^2 + 2t_2^2 + 3t_1 t_2\right)}, \quad (2)$$

where R is the radius of the tube, E_1, E_2 denote the elastic modulus, t_1, t_2 demote the thickness, and η_1, η_2 denote the multiplier which equals $1 + \nu_1$ and $1 + \nu_2$, where ν is Poisson's ratio, and $\varepsilon_1^0, \varepsilon_2^0$ denote the initial strain for each layer before rolling up, respectively. From Eq. (2), the difference in initial strain between the two layers determines the final radius of the rolled-up structures.[52] Unfortunately, directly measuring the initial strain in the bilayers is difficult because the sacrificial layer (PMMA) is unstable under intense focused nanobeam illumination used for strain mapping. Instead, we measure the residual strain in the rolled tube structure using position-sensitive NBED technique. This approach provides valuable insight into the evolution of the strain distribution within the nanomembrane system during the process of releasing and rolling.

Similar to the case of the bilayer model,[51] the nanomembrane is thin enough compared to its length and width. Thus, the residual strain being investigated is mainly the tangential strain, ε_{xx}, which is along the rolling up direction [see Eq. (1)]. This could be measured using NBED in the cross-sectional view of FIB-prepared samples [Figs. 1(c) and 1(d)]. We conduct NBED experiments on a Talos F200i (Thermo Fischer Scientific) field emission S/TEM operated at 200 kV. The NBED patterns are collected in STEM mode, with a semi-convergent angle of the probe forming lens setting to 0.60 mrad (probe size on sample plane $d_{probe} \approx 2.15$ nm). The diffraction patterns are recorded with a CETA 16M scintillator-based CMOS camera with 4096×4096 pixels. To improve the accuracy of NBED strain mapping, we pre-calibrated the optical parameters of the microscope before the diffraction experiments. We first calibrate the relative rotations between the CMOS camera and the HAADF images using a [110] zone axis single crystal Si sample (Fig. S3). We also use the diffraction pattern from the single crystal to calibrate the camera length (Fig. S3). The diffraction distortion introduced by the diffraction lens system is also calibrated using electron diffraction from an unstrained amorphous SiO$_2$ cross-sectional sample (Fig. S4).

The diffraction pattern of amorphous SiO/SiO$_2$ rolled-up nanomembranes exhibits a characteristic diffused ring, as shown in Fig. 2(a). Compared to parallel electron beam diffraction, the NBED pattern is formed by convolving the reciprocal structure with the aperture function of the probe-forming lens. However, this convolution would not affect the peak intensity position q_{peak}. When strain is present, the locations of q_{peak} will slightly move along the radial direction with varying azimuth angles ϑ. $q_{peak}(\vartheta)$ then forms an ellipse instead of a circle [Fig. 1(e)] in each of NBED pattern. We subsequently extract the local residual strain ε of the amorphous bilayers from the ellipticity of NBED patterns ϵ as follows:

$$\varepsilon = \frac{q_0 - q(\vartheta)}{q_0} = \epsilon = \frac{a - c}{a} \times 100\%, \quad (3)$$
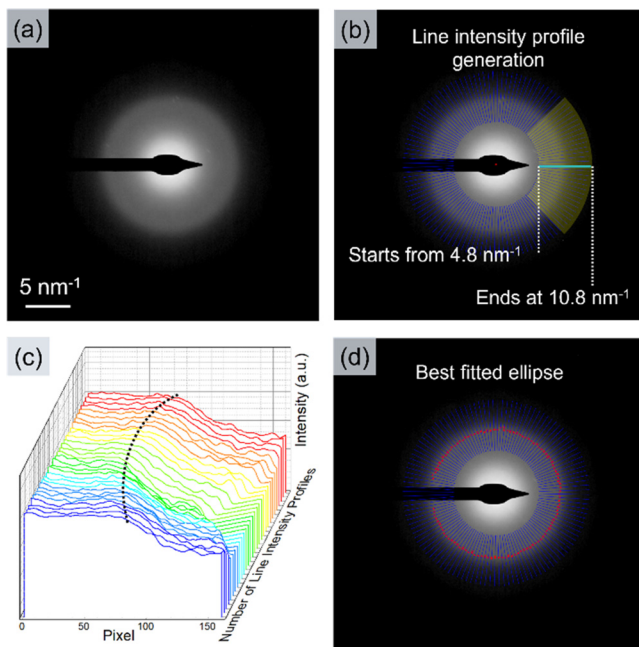
FIG. 2. NBED data processing and best-ellipse fitting for strain mapping. (a) An experimental NBED pattern of the amorphous SiO/SiO$_2$ sample. (b) Line profiles (blue lines) across the diffuse ring for intensity peak finding. Each line profile starts from 4.8 nm^{-1} and ends at 10.8 nm^{-1}. (c) Plot of the intensity line profiles extracted from the yellow shaded regions in (b), the black dashed line marks the found peak intensity q_{peak}. (d) The red circle shows the best-fitted ellipse formed with q_{peak} at different azimuth angles.

where a and c are the length of the major and minor axes of the fitted ellipse, respectively. It should be noted that this is only a simple estimate of uniaxial strain that applies to the current rolling up structures. The strain is dominated by the component along the tangential direction of the nanotube. For generic amorphous materials, a comprehensive strain determination should be accomplished by comparing the fitted ellipse to a circle with radius q_0, which could be derived from NBED patterns recorded in a strain-free region, used as a reference state.

In Fig. 2(b), the diffused ring is segmented by 120 lines starting from the center of the diffraction pattern. We calibrate the origin point of the diffraction pattern by analyzing the symmetry of the intensity line profile pairs with opposite directions. If the origin is incorrect, the intensity profiles in pairs will not be symmetrically distributed (Fig. S5). To address this issue, we offset the initial coordinates of the origin and extract intensity line profiles. We repeat this process for multiple azimuth angles until the line profile shapes are symmetrically distributed around the origin, whenever strain exists. To mitigate the impact of the beam stopper blockage, we limit the plotted intensity line profile to the range of 4.8–10.8 nm^{-1}. This allows us to identify the $q_{peak}(\vartheta)$ in each line profile. Figure 2(c) shows the series of line intensity profiles taken from the region highlighted in Fig. 2(b). Figure 2(d) depicts the circle formed by the points corresponding to the characteristic diffraction peaks $q(\vartheta)$. With the coordinates of points corresponding to $q(\vartheta)$ extracted, the ellipse is fitted by the least-square

method as reported.[53] We have included the MATLAB codes for peak finding, extraction, and ellipse fitting in the supplementary material (Fig. S6).

We first conduct NBED strain mapping on the wet-etched, particle-free, rolled-up nanomembrane, and Fig. 3 shows the results. The white-dashed boxes in the HAADF image [Fig. 3(a)] show the specific ROIs under investigation for NBED strain mapping. For each specific ROI, the dimension is 25×25 nm^2. Within each ROI, the nanobeam is scanned over 80–100 spots. All the recorded NBED patterns are then summed together for ellipse fitting, which improves the signal-to-noise ratio. The strain in a rolled-up nanomembrane consisting of two layers of Si$_3$N$_4$ has been analyzed, and the results are presented in Fig. 3(b). The inner layer (spot series 1) exhibits an average residual strain of 0.54%, while the outer layer (spot series 2) has an average residual strain of 0.45%. The average strain for both layers combined is 0.49%. The inner layer exhibits slightly higher residual strain, which is consistent with its smaller radius. According to the uniaxial strain model, the dominant tangential strain in these self-rolling nanostructures follows either the long or short axis of the ellipses. Experimental results show that the long axis of the ellipses aligns with the nanoribbon's bending direction. This indicates the validation of the uniaxial strain model and further reveals that the nanotube is under tensile strain along the circumferential direction, as shown by the yellow arrows in Fig. 4.

We then apply the scanning NBED strain mapping method to the dry-released rolled-up amorphous nanomembrane. Figure 4(a) shows the cross-sectional view of the sample, while Pd particles show brighter contrast. The Pd particles are ∼5 nm in diameter and randomly distributed on the nanomembrane surface. The rolled-up nanomembrane has a radius of ∼650 nm, with uniform shape and curvature. The sample is divided into 10 radial segments (marked by colored boxes), as in a clock. Figures 4(b)–4(k) show the close-up look of sub-ROIs (marked by dashed white squares) in each radial segment, and the size of the sub-ROIs is 5×5 nm^2. We use these sub-regions to measure strain to exclude the Pd particles. The orange arrows clearly indicate that the direction of strains measured within the rolled-up nanomembrane follows the tangential direction of the circumferential cross section, which is consistent with the expected strain distributions in a rolled-up sample. Since the long axis of the ellipses aligns with the circumferential direction, tensile strain is present there. In Fig. 4(i), we also measure the magnitude of the strain in each sub-ROI, and the overall average magnitude of the residual strain for this sample is 0.81%. Deviations in the direction of the strain come from the anisotropic strain around the Pd nanoparticle, as does the fluctuation in the measured strain magnitude from each sub-ROI.

The average magnitude of the tangential strain in the Pd-assistant SiO/SiO$_2$ sample is larger than that in the pure Si$_3$N$_4$ sample. The surface tension of the Pd nanoparticle during solidification exerts an external force on nearby regions, contributing to the strain along the tangential direction of the rolled-up structure. Previous studies on rolled-up nanomembranes have found it challenging to achieve radii as small as 100–1000 nm using only intrinsic strain, without the assistance of metal nanoparticles.[39] The difference in the measured residual strains indicates that the metal nanoparticles do increase the tangential strain, and potentially the strain gradient, thereby enabling the creation of rolled-up amorphous structures with a smaller radius. In our experiments, we used a uniaxial model to extract the strain information from
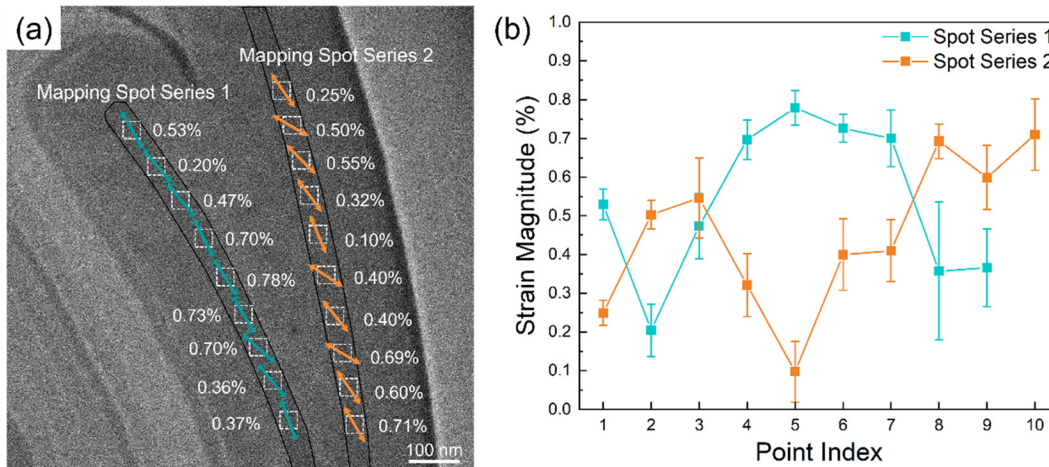
20 March 2024 08:34:19

FIG. 3. NBED strain mapping of rolled-up amorphous Si_3N_4 nanomembranes. (a) The magnified HAADF-STEM image shows the two rolled-up Si_3N_4 layers marked by the black boxes. Multiple NBED patterns are summed within each white box to improve the signal-to-noise ratio for strain measurement. Orange and green arrows indicate the determined directions of local elastic strain, with corresponding values. (b) Measured strain magnitude of the two series in (a).
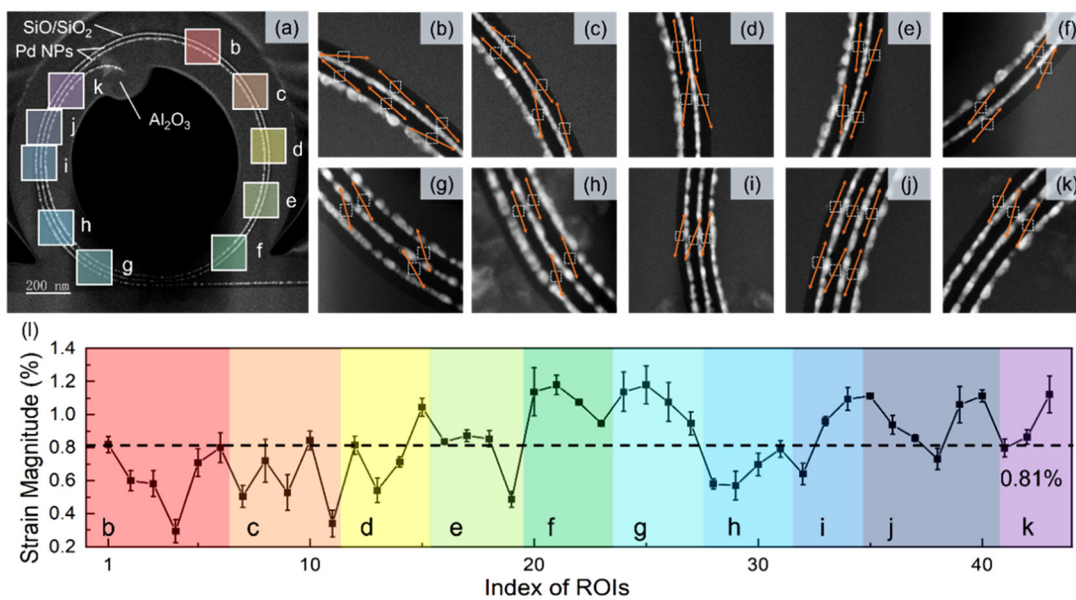

FIG. 4. NBED strain mapping of the rolled-up amorphous SiO/SiO_2 nanomembrane. (a) A cross section view of the sample captured using HAADF-STEM imaging. White rectangles indicate the regions of interest (ROI) for NBED mapping. (b)–(k) Yellow arrows indicate the determined directions of local elastic strain. (l) The measured strain magnitude from the corresponding ROIs. Each dot represents data from a sub-region [white boxes in (b)–(k)] to exclude Pd particles.

the axial directions of the ellipse, taking advantage of the intrinsic property of the self-rolling nanostructures. For generic amorphous materials, if a strain-free region could be found to provide a q_0 value as reference state, it is possible to extract more compressive strain information from the NBED by comparing the ellipse with the circle extracted from the strain-free regions.

In conclusion, we have measured the local elastic strains in amorphous rolled-up nanomembranes at the nanoscale using NBED. We relate real space strain with anisotropy in reciprocal space. We apply the method to two rolled-up amorphous nanomembranes. The results show consistency between the direction of local tangential strain and the rolling geometry of the sample. The residual strain in the two samples differs noticeably not only due to the choice of different materials but, more importantly, due to the strain enhancement caused by the presence of metal nanoparticles. The present results demonstrate the feasibility of nanoscale strain mapping in amorphous specimens with complex 3D structures, providing solutions for high-resolution strain distribution characterization in flexible electronics. The quantitative

measurement of local strain enables greater insight into the rolling process of membranes on the nanoscale.

See the supplementary material for the STEM images of the rolled-up nanomembrane sample, the calibration procedures for the strain measurement, and MATLAB code for peak finding, extraction, and ellipse fitting.

AUTHOR DECLARATIONS
Conflict of Interest

The authors have no conflicts to disclose.

Author Contributions

Zhi Zheng: Conceptualization (equal); Data curation (lead); Formal analysis (lead); Investigation (lead); Methodology (lead); Validation (equal); Visualization (lead); Writing – original draft (lead); Writing – review & editing (equal). **Chang Liu:** Formal analysis (supporting); Methodology (supporting). **Wenhao He:** Formal analysis (supporting); Methodology (supporting). **Jiayuan Huang:** Methodology (supporting). **Jiachuo He:** Methodology (supporting). **GaoShan Huang:** Funding acquisition (equal); Validation (equal); Writing – review & editing (equal). **Yongfeng Mei:** Conceptualization (equal); Funding acquisition (equal); Validation (equal); Writing – review & editing (equal). **Changlin Zheng:** Conceptualization (equal); Funding acquisition (equal); Validation (equal); Writing – review & editing (equal).

DATA AVAILABILITY

The data that support the findings of this study are available from the corresponding authors upon reasonable request.

REFERENCES

[1] B. D. Gates, "Flexible electronics," Science **323**(5921), 1566–1567 (2009).

[2] M. Kaltenbrunner, T. Sekitani, J. Reeder, T. Yokota, K. Kuribara, T. Tokuhara, M. Drack, R. Schwödiauer, I. Graz, and S. Bauer-Gogonea, "An ultra-lightweight design for imperceptible plastic electronics," Nature **499**(7459), 458–463 (2013).

[3] F. Faisal, Y. Amin, Y. Cho, and H. Yoo, "Compact and flexible novel wideband flower-shaped CPW-fed antennas for high data wireless applications," IEEE Trans. Antennas Propag. **67**(6), 4184–4188 (2019).

[4] Y. Khan, A. Thielens, S. Muin, J. Ting, C. Baumbauer, and A. C. Arias, "A new frontier of printed electronics: Flexible hybrid electronics," Adv. Mater. **32**(15), 1905279 (2020).

[5] J. A. Rogers, M. G. Lagally, and R. G. Nuzzo, "Synthesis, assembly and applications of semiconductor nanomembranes," Nature **477**(7362), 45–53 (2011).

[6] A. Nathan, A. Ahnood, M. T. Cole, S. Lee, Y. Suzuki, P. Hiralal, F. Bonaccorso, T. Hasan, L. Garcia-Gancedo, A. Dyadyusha, S. Haque, P. Andrew, S. Hofmann, J. Moultrie, D. Chu, A. J. Flewitt, A. C. Ferrari, M. J. Kelly, J. Robertson, G. A. J. Amaratunga, and W. I. Milne, "Flexible electronics: The next ubiquitous platform," Proc. IEEE **100**, 1486–1517 (2012).

[7] D. Corzo, G. Tostado-Blázquez, and D. Baran"Flexible electronics: Status, challenges and opportunities," Front. Electron. **1**, 594003 (2020).

[8] S. R. Forrest, "The path to ubiquitous and low-cost organic electronic appliances on plastic," Nature **428**(6986), 911–918 (2004).

[9] K. Zhang, J.-H. Seo, W. Zhou, and Z. Ma, "Fast flexible electronics using transferrable silicon nanomembranes," J. Phys. D **45**(14), 143001 (2012).

[10] H. Sirringhaus, T. Kawase, R. H. Friend, T. Shimoda, M. Inbasekaran, W. Wu, and E. P. Woo, "High-resolution inkjet printing of all-polymer transistor circuits," Science **290**(5499), 2123–2126 (2000).

[11] G. H. Gelinck, H. E. A. Huitema, E. van Veenendaal, E. Cantatore, L. Schrijnemakers, J. B. P. H. van der Putten, T. C. T. Geuns, M. Beenhakkers, J. B. Giesbers, B.-H. Huisman, E. J. Meijer, E. M. Benito, F. J. Touwslager, A. W. Marsman, B. J. E. van Rens, and D. M. de Leeuw, "Flexible active-matrix displays and shift registers based on solution-processed organic transistors," Nat. Mater. **3**(2), 106–110 (2004).

[12] J. Yoon, S. Jo, I. S. Chun, I. Jung, H.-S. Kim, M. Meitl, E. Menard, X. Li, J. J. Coleman, U. Paik, and J. A. Rogers, "GaAs photovoltaics and optoelectronics using releasable multilayer epitaxial assemblies," Nature **465**(7296), 329–333 (2010).

[13] H.-X. Ji, X.-L. Wu, L.-Z. Fan, C. Krien, I. Fiering, Y.-G. Guo, Y. Mei, and O. G. Schmidt, "Self-wound composite nanomembranes as electrode materials for lithium ion batteries," Adv. Mater. **22**(41), 4591–4595 (2010).

[14] J. Wang, T. Zhan, G. Huang, X. Cui, X. Hu, and Y. Mei, "Tubular oxide microcavity with high-index-contrast walls: Mie scattering theory and 3D confinement of resonant modes," Opt. Express **20**(17), 18555–18567 (2012).

[15] E. J. Smith, Z. Liu, Y. Mei, and O. G. Schmidt, "Combined surface plasmon and classical waveguiding through metamaterial fiber design," Nano Lett. **10**(1), 1–5 (2010).

[16] Y. Mei, A. A. Solovev, S. Sanchez, and O. G. Schmidt, "Rolled-up nanotech on polymers: From basic perception to self-propelled catalytic microengines," Chem. Soc. Rev. **40**(5), 2109–2119 (2011).

[17] A. A. Solovev, W. Xi, D. H. Gracias, S. M. Harazim, C. Deneke, S. Sanchez, and O. G. Schmidt, "Self-propelled nanotools," ACS Nano **6**(2), 1751–1756 (2012).

[18] Y. Mei, G. Huang, A. A. Solovev, E. B. Ureña, I. Mönch, F. Ding, T. Reindl, R. K. Y. Fu, P. K. Chu, and O. G. Schmidt, "Versatile approach for integrative and functionalized tubes by strain engineering of nanomembranes on polymers," Adv. Mater. **20**(21), 4085–4090 (2008).

[19] R. Bierwolf, M. Hohenstein, F. Phillipp, O. Brandt, G. E. Crook, and K. Ploog, "Direct measurement of local lattice distortions in strained layer structures by HREM," Ultramicroscopy **49**(1), 273–285 (1993).

[20] A. Rosenauer, *Transmission Electron Microscopy of Semiconductor Nanostructures: An Analysis of Composition and Strain State* (Springer Science & Business Media, 2003).

[21] P. L. Galindo, A. Yáñez, J. Pizarro, E. Guerrero, T. Ben, and S. I. Molina, in *Microscopy of Semiconducting Materials*, edited by A. G. Cullis and J. L. Hutchison (Springer, Berlin, Heidelberg, 2005), pp. 191–194.

[22] W. Neumann, H. Kirmse, I. Häusler, and R. Otto, "Quantitative high resolution transmission electron microscopy of nanostructured semiconductors," J. Microsc. **223**(3), 200–204 (2006).

[23] F. Hüe, M. Hÿtch, H. Bender, F. Houdellier, and A. Claverie, "Direct mapping of strain in a strained silicon transistor by high-resolution electron microscopy," Phys. Rev. Lett. **100**(15), 156602 (2008).

[24] C. T. Koch, V. B. Özdöl, and P. A. van Aken, "An efficient, simple, and precise way to map strain with nanometer resolution in semiconductor devices," Appl. Phys. Lett. **96**(9), 091901 (2010).

[25] A. Béché, J. L. Rouvière, J. P. Barnes, and D. Cooper, "Strain measurement at the nanoscale: Comparison between convergent beam electron diffraction, nano-beam electron diffraction, high resolution imaging and dark field electron holography," Ultramicroscopy **131**, 10–23 (2013).

[26] J. L. Rouvière, A. Mouti, and P. Stadelmann, "Measuring strain on HR-STEM images: Application to threading dislocations in $Al_{0.8}In_{0.2}N$," J. Phys.: Conf. Ser. **326**(1), 012022 (2011).

[27] L. Jones, S. Wenner, M. Nord, P. H. Ninive, O. M. Løvvik, R. Holmestad, and P. D. Nellist, "Optimising multi-frame ADF-STEM for high-precision atomic-resolution strain mapping," Ultramicroscopy **179**, 57–62 (2017).

[28] Q. Li, T. Miao, H. Zhang, W. Lin, W. He, Y. Zhong, L. Xiang, L. Deng, B. Ye, Q. Shi, Y. Zhu, H. Guo, W. Wang, C. Zheng, L. Yin, X. Zhou, H. Xiang, and J.

Shen, "Electronically phase separated nano-network in antiferromagnetic insulating LaMnO₃/PrMnO₃/CaMnO₃ tricolor superlattice," Nat. Commun. **13**(1), 6593 (2022).

[29]M. J. Hÿtch, "Geometric phase analysis of high resolution electron microscope images," Scanning Microsc. **11**, 53–66 (1997).

[30]P. L. Galindo, S. Kret, A. M. Sanchez, J.-Y. Laval, A. Yáñez, J. Pizarro, E. Guerrero, T. Ben, and S. I. Molina, "The Peak Pairs algorithm for strain mapping from HRTEM images," Ultramicroscopy **107**(12), 1186–1193 (2007).

[31]V. B. Ozdol, C. Gammer, X. G. Jin, P. Ercius, C. Ophus, J. Ciston, and A. M. Minor, "Strain mapping at nanometer resolution using advanced nano-beam electron diffraction," Appl. Phys. Lett. **106**(25), 253107 (2015).

[32]G. W. Paterson, R. W. H. Webster, A. Ross, K. A. Paton, T. A. Macgregor, D. McGrouther, I. MacLaren, and M. Nord, "Fast pixelated detectors in scanning transmission electron microscopy. Part II: Post-acquisition data processing, visualization, and structural characterization," Microsc. Microanal. **26**(5), 944–963 (2020).

[33]D. Yoon, K. Harikrishnan, Y.-T. Shao, and D. A. Muller, "High-speed, high-precision, and high-throughput strain mapping with cepstral transformed 4D-STEM Data," Microsc. Microanal. **28**(S1), 796–798 (2022).

[34]M. Hÿtch, F. Houdellier, F. Hüe, and E. Snoeck, "Nanoscale holographic interferometry for strain measurements in electronic devices," Nature **453**(7198), 1086–1089 (2008).

[35]D. Cooper, J.-P. Barnes, J.-M. Hartmann, A. Béché, and J.-L. Rouvière, "Dark field electron holography for quantitative strain measurements with nanometer-scale spatial resolution," Appl. Phys. Lett. **95**(5), 053501 (2009).

[36]A. Béché, J. L. Rouvière, J. P. Barnes, and D. Cooper, "Dark field electron holography for strain measurement," Ultramicroscopy **111**(3), 227–238 (2011).

[37]C. Gammer, C. Ophus, T. C. Pekin, J. Eckert, and A. M. Minor, "Local nanoscale strain mapping of a metallic glass during in situ testing," Appl. Phys. Lett. **112**(17), 171905 (2018).

[38]S. Kang, D. Wang, A. Caron, C. Minnert, K. Durst, C. Kübel, and X. Mu, "Direct observation of quadrupolar strain fields forming a shear band in metallic glasses," Adv. Mater. **35**(25), 2212086 (2023).

[39]J. Li, J. Zhang, W. Gao, G. Huang, Z. Di, R. Liu, J. Wang, and Y. Mei, "Dry-released nanotubes and nanoengines by particle-assisted rolling," Adv. Mater. **25**(27), 3715–3721 (2013).

[40]S. Kang, D. Wang, C. Kübel, and X. Mu, "Importance of TEM sample thickness for measuring strain fields," Ultramicroscopy **255**, 113844 (2024).

[41]B. Wu, Z. Zhang, B. Chen, Z. Zheng, C. You, C. Liu, X. Li, J. Wang, Y. Wang, E. Song, J. Cui, Z. An, G. Huang, and Y. Mei, "One-step rolling fabrication of VO₂ tubular bolometers with polarization-sensitive and omnidirectional detection," Sci. Adv. **9**(42), eadi7805 (2023).

[42]B. Wu, Z. Zhang, Z. Zheng, T. Cai, C. You, C. Liu, X. Li, Y. Wang, J. Wang, H. Li, E. Song, J. Cui, G. Huang, and Y. Mei, "Self-rolled-up ultrathin single-crystalline silicon nanomembranes for on-chip tubular polarization photodetectors," Adv. Mater. **35**, 2306715 (2023).

[43]W. Huang, X. Yu, P. Froeter, R. Xu, P. Ferreira, and X. Li, "On-chip inductors with self-rolled-up SiNₓ nanomembrane tubes: A novel design platform for extreme miniaturization," Nano Lett. **12**(12), 6283–6288 (2012).

[44]W. Huang, J. Zhou, P. J. Froeter, K. Walsh, S. Liu, M. D. Kraman, M. Li, J. A. Michaels, D. J. Sievers, S. Gong, and X. Li, "Three-dimensional radio-frequency transformers based on a self-rolled-up membrane platform," Nat. Electron. **1**(5), 305–313 (2018).

[45]W. Huang, Z. Yang, M. D. Kraman, Q. Wang, Z. Ou, M. M. Rojo, A. S. Yalamarthy, V. Chen, F. Lian, J. H. Ni, S. Liu, H. Yu, L. Sang, J. Michaels, D. J. Sievers, J. G. Eden, P. V. Braun, Q. Chen, S. Gong, D. G. Senesky, E. Pop, and X. Li, "Monolithic mtesla-level magnetic induction by self-rolled-up membrane technology," Sci. Adv. **6**(3), eaay4508 (2020).

[46]C. Ebner, R. Sarkar, J. Rajagopalan, and C. Rentenberger, "Local, atomic-level elastic strain measurements of metallic glass thin films by electron diffraction," Ultramicroscopy **165**, 51–58 (2016).

[47]D. Yu-Fu, Y. Fei, Y. Jian-Lin, and Z. Wei, "The increasing of localized free volume in bulk metallic glass under uniaxial compression," Chin. Phys. **16**(7), 2051 (2007).

[48]Y. H. Li, W. Zhang, C. Dong, J. B. Qiang, K. Yubuta, A. Makino, and A. Inoue, "Unusual compressive plasticity of a centimeter-diameter Zr-based bulk metallic glass with high Zr content," J. Alloys Compd. **504**, S2–S5 (2010).

[49]E. Abe, "Atomic-scale characterization of nanostructured metallic materials by HAADF/Z-contrast STEM," Mater. Trans. **44**(10), 2035–2041 (2003).

[50]X. Mu, D. Wang, T. Feng, and C. Kübel, "Radial distribution function imaging by STEM diffraction: Phase mapping and analysis of heterogeneous nanostructured glasses," Ultramicroscopy **168**, 1–6 (2016).

[51]G. P. Nikishkov, "Curvature estimation for multilayer hinged structures with initial strains," J. Appl. Phys. **94**(8), 5333–5336 (2003).

[52]L. Wang, Z. Tian, B. Zhang, B. Xu, T. Wang, Y. Wang, S. Li, Z. Di, and Y. Mei, "On-chip rolling design for controllable strain engineering and enhanced photon–phonon interaction in graphene," Small **15**(23), 1805477 (2019).

[53]A. Fitzgibbon, M. Pilu, and R. B. Fisher, "Direct least square fitting of ellipses," IEEE Trans. Pattern Anal. Mach. Intell. **21**(5), 476–480 (1999).

20 March 2024 08:34:19